DESIGN OF A FLEXURE-BASED DYNAMIC-TUNABLE FIVE-AXIS NANOPOSITIONER

Chenglin Li, Ji Wang, and Shih-Chi Chen*
Department of Mechanical and Automation Engineering
The Chinese University of Hong Kong
Shatin, N.T., Hong Kong SAR, China
*Email:scchen@mae.cuhk.edu.hk

In this paper, we present the development of a flexure-based five-axis nanopositioner with dynamic-tuning capability for parallel nanomanufacturing applications, e.g. electro-machining (nano-EM), dip-pen nanolithography and nano-scratching. Static, dynamic, and dynamic-tuning experiments were devised and performed to characterize the range, speed, and resolution characteristics of the nanopositioner.

DYNAMIC-TUNING FOR NANOPOSITIONER

Nanopositioners can move objects of different sizes with nanometer precision. They are important as they set the limits on our ability to measure, manipulate, and manufacture physical systems. To fulfill the stringent repeatability and precision requirements, compliant mechanisms, i.e. flexures, are often used for their advantages (no wear between joint members and free of backlash etc.) over traditional mechanical linkages [1].

It is known that the dynamic performance of a flexural mechanism depends on its natural frequency; however, this is often compromised by the required stroke of the mechanism. In other words, high natural frequency can only be achieved at the expense of reduced stroke. In this work, we aim to develop a dynamic-tunable flexure-based nanopositioner that allows trade-offs between its speed (natural frequency) and range (stroke)—a concept inspired by compliant actuators used in humanoid robots [2].

The dynamic-tuning effect is achieved by exploiting the "stress-stiffening effect", i.e. the stiffness of a beam increases when it experiences tensile loads in the axial direction [3]. The natural frequency of a simply supported beam with axial force N can be described by Equation (1), where ω is the natural frequency; l, A, I, E, ρ is the length, cross section area, moment of inertia, Young's modulus, density of the beam, respectively [3]. For example, the natural frequency of a 70mm long and 1mm thick titanium beam can be shifted from 450Hz to 1164Hz when 1000N tensile force is applied. Note that compression load is not used as it may cause buckling and instability.

$$\omega = \left(\frac{\pi}{l}\right)^2 \sqrt{\frac{EI}{\rho A}} \sqrt{1 + \frac{Nl^2}{\pi^2 EI}} \quad (1)$$

Figure 1 presents the simulated results of a symmetric double parallelogram (DP) mechanism with increasing axial loads until the yield stress is reached. Figure 1A shows the CAD model. The material used in the FEA simulation is titanium.

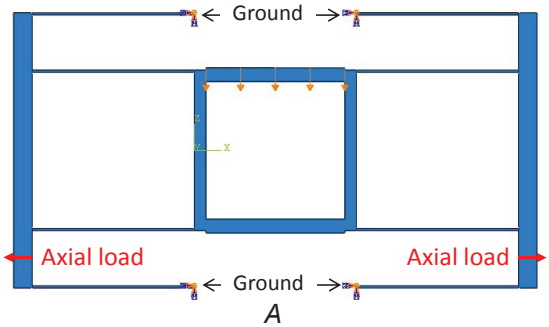

A

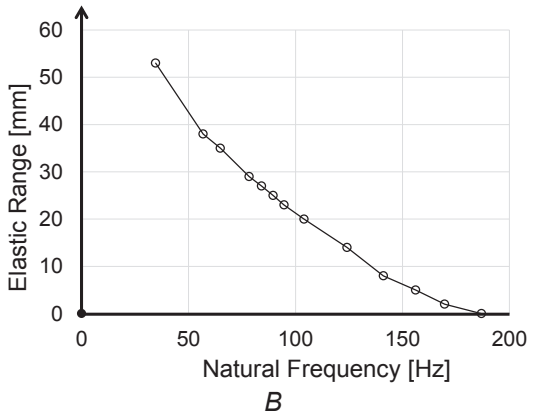

B

FIGURE 1. Simulated results of a symmetric DP flexure using Abaqus 6.12. A: CAD model with load and boundary conditions; B: The relationship between range and frequency

NANOPOSITIONER DESIGN

Figure 2 shows the layout of the nanopositioner, where an in-plane X-Y stage and an out-of-plane Z-θ_X-θ_Y stage are connected in series to achieve five degrees of freedom. The design of the X-Y stage utilizes the principle of constraint-based design [4] by using multiple folded-beam mechanisms to decouple the X and Y motion. The extended range in the X and Y directions are achieved by the symmetric DP mechanism. To implement dynamic-tuning, two piezoelectric actuators (green arrows in Figure 2; PI P-845.20) are used in each DP mechanism to generate axial loads (stress) for dynamic-tuning. The dynamic-tuning design is implemented on the X-Y stage to enable trade-offs between its range and speed.

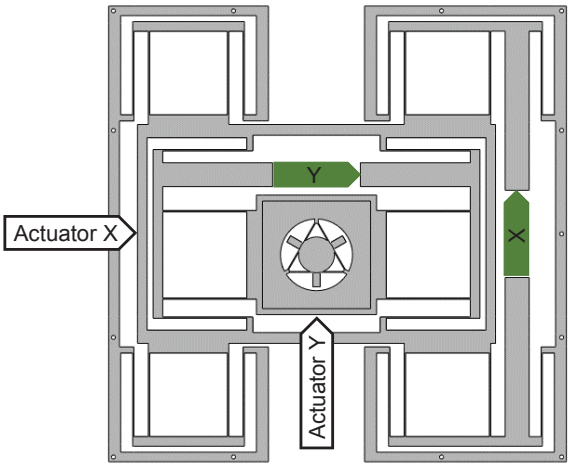

FIGURE 2. Layout of the nanopositioner. Green arrows indicate the piezoelectric actuators (PI P-845.20) for stiffness-tuning; white arrows indicate the linear actuators (PI M-230.10) for in-plane actuation.

Figure 3 shows the layout of the out-of-plane compliant stage which generates independent motions in the Z, θ_X, and θ_Y directions. The central stage is supported by six flexural arms. Three piezoelectric actuators (Newport NPA100) are installed below the motion tabs extending from the central stage, as indicated by the blue circles. Three capacitance probes (in red; Lion Precision C30/CPL290) are used to measure the out-of-plane displacements for closed-loop position control. Piezoelectric actuators are used for the out-of-plane stage for high-speed parallelism control and nano-patterning application.

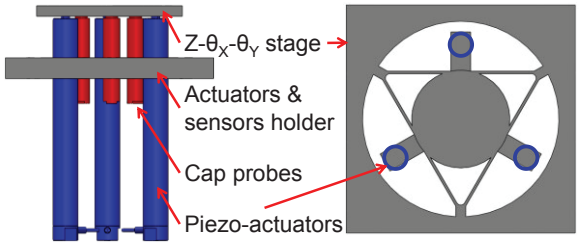

FIGURE 3. Z-θ_X-θ_Y stage with integrated actuators and sensors (Newport NPA100 and Lion Precision C30). A: Side view; B: Top view

ASSEMBLY AND CHARACTERIZATION

Figure 4 shows the five-axis nanopositioner prototype with integrated actuators and sensors.

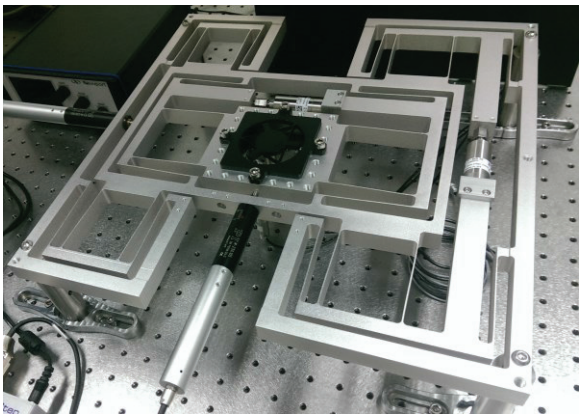

FIGURE 4. Prototype of the five-axis nanopositioner

To characterize the dynamic properties of the nanopositioner, we first conducted an impulse response experiment to obtain resonant frequencies of the nanopositioner in different axes. Resonant frequencies were calculated from the displacement data by performing the fast Fourier transform (FFT). Table 1 summarizes the measured and simulated resonant frequencies. These parameters are used in the dynamic-tuning experiments as well as the implementation of closed-loop control.

TABLE 1. Natural frequencies of the five-axis nanopositioner

Freq [Hz]	X	Y	Z	θ_X	θ_Y
Simulated	15.5	20.1	2236	3499	3558
Measured	14.5	20.3	1936	3223	3182

To understand the level of cross-axis motion coupling and implement the open-loop control, static displacement experiments were performed

to identify the input-output matrix $\boldsymbol{S_X}$ that maps actuator displacements to mechanism displacements. Equations (2) and (3) [5] are used to obtain the matrix $\boldsymbol{S_X}$. The measured results are shown in Equation (4).

$$X_C = S_X X_A \rightarrow \begin{bmatrix} \Delta x & \Delta y & \Delta z & \Delta\theta_x & \Delta\theta_y \end{bmatrix}^{\mathrm{T}} = S_X \begin{bmatrix} x & y & z_1 & z_2 & z_3 \end{bmatrix}^{\mathrm{T}} \quad (2)$$

$$X_A = S_X^{-1} X_C \quad (3)$$

$$S_X = \begin{bmatrix} 0.950 & -0.011 & -0.002 & -0.001 & -0.002 \\ -0.008 & 0.987 & -0.038 & -0.033 & -0.002 \\ 0.002 & 0.001 & 0.105 & 0.157 & 0.108 \\ 0 & 0 & 0 & -0.013 & 0.010 \\ 0 & 0 & -0.011 & 0.004 & 0.007 \end{bmatrix} \quad (4)$$

POSITIONGING EXPERIMENT

First, static positioning experiments in selected axes (X, Z, and θ_X) were performed to demonstrate the range and precision of the nanopositioner. In these experiments, the input-output matrix, $\boldsymbol{S_X}$, was used as an open-loop controller. Figure 5 shows the measured displacements and rotation in the X, Z and θ_X axis respectively. The displacements and rotation are plotted versus open-loop displacement commands in the left column, and the off-axis errors are plotted versus displacement commands in the right column. Overall, we found the off-axis parasitic motions to be reasonably small, i.e. 0.05% of the device's range.

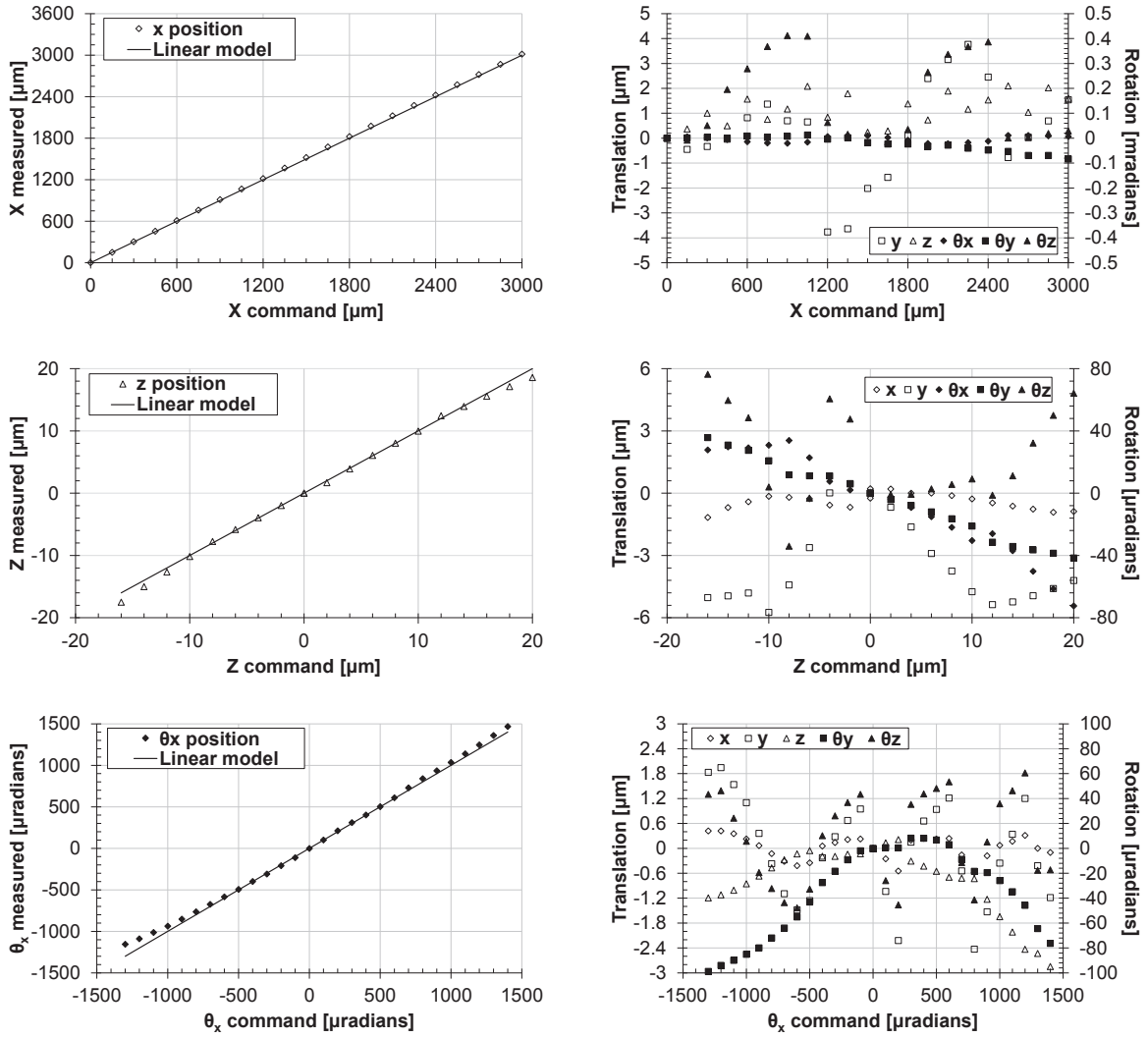

FIGURE 5. X, Z, and θ_X position results

In the second experiment, the nanopositioner was commanded to generate precise X and Z motions with the open-loop controller in a local work volume to demonstrate its nanoscale positioning capability. Figure 6 plots the measured displacements (left) and off-axis errors (right) versus open-loop displacement commands. The results demonstrate the nanopositioner can precisely perform multi-axis nano-patterning tasks with 10s nanometer precision. The precision can be further improved with closed-loop control.

DYNAMIC-TUNING EXPERIMENT

To validate the in-plane dynamic-tuning capability, axial loads (displacements) were applied to the X-Y stage by the stiffness-tuning actuators shown in Figure 2. The results are shown in Figure 7, where resonant frequencies in X and Y directions can be increased by 2-3 times with increasing axial loading. The measured resonant frequencies are constantly lower than the simulated results and the errors increase with increasing displacements. This may be due to the following reasons: (1) misalignment between the piezoelectric actuator and the loading axis and (2) imperfect actuator constraints.

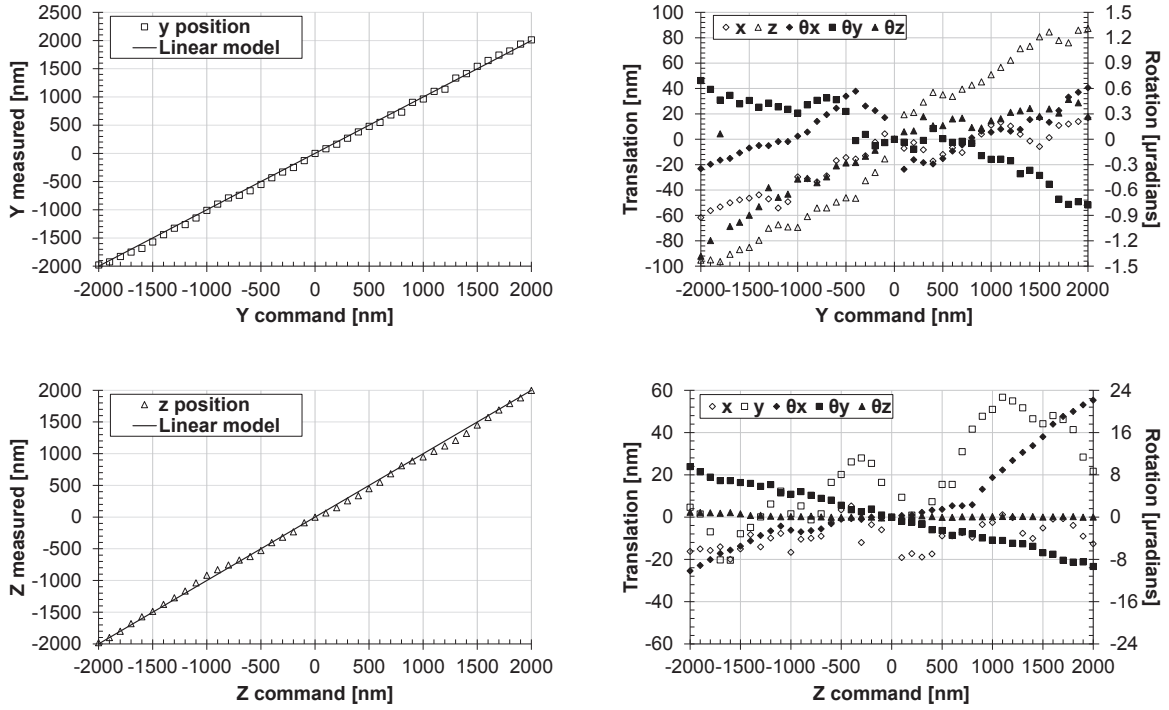

FIGURE 6. Y and Z position results

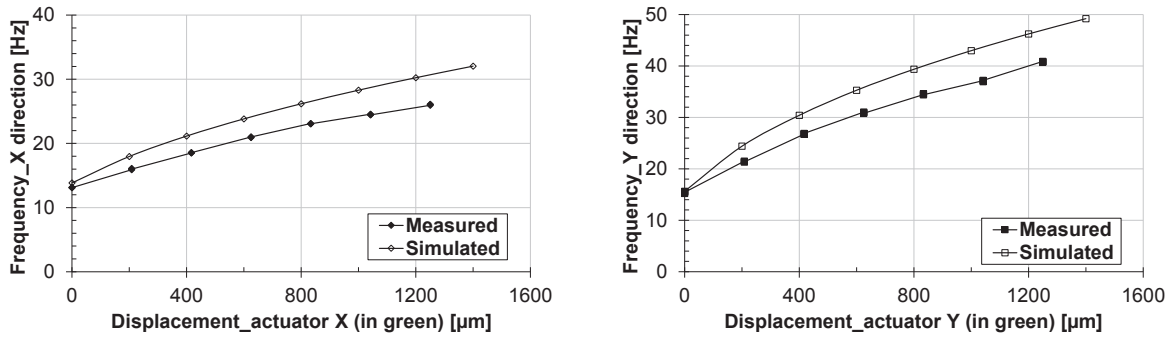

FIGURE 7. The relationship between resonant frequency and applied displacement

NANOMANUFACTURING STATION

Figure 8 presents the conceptual design of a nanomanufacturing station design that includes the five-axis nanopositioner integrated with a custom-built AFM tip/stage assembly, where an AFM tip array is affixed to a manual Z-positioner with a side imaging camera that provides coarse distance control between the AFM tips and the sample. During a nano-patterning process, the $Z\text{-}\theta_X\text{-}\theta_Y$ stage controls both the Z position of the tip array and the parallelism between the array and the sample, while the X-Y stage performs the actual X-Y scanning and patterning.

When the area to be patterned is smaller than the default range of the X-Y stage, the stiffness-tuning commences. According to the FEA results in Figure 1B, the natural frequency of the X-Y stage can be easily increased by a factor of 2 to achieve higher patterning speed and better dynamic characteristics.

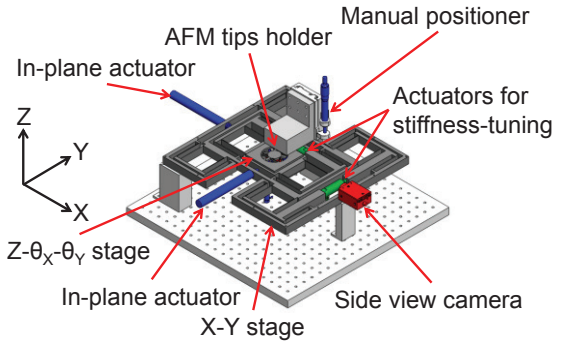

FIGURE 8. CAD model of the nano-manufacturing station

CONCLUSION

We have developed a dynamic-tunable five-axis nanopositioner. In this paper, we presented the design, modeling, assembly, and characterization of the nanopositioner, including the static, dynamic, and frequency-tuning characteristics. Our experiments indicate the nanopositioner can control the stage position within ±25nm and tune its natural frequency between 15 to 40 Hz, which proves effective trade-offs between the natural frequency and elastic range. The demonstrated range and precision make the five-axis nanopositioner suitable for various large area parallel nanomanufacturing applications, including nano-EM, dip-pen nanolithography and nano-scratching. A parallel nanomanufacturing station will be developed based on the nanopositioner and a custom-developed AFM.

ACKNOWLEDGEMENT

This work is supported by the HKSAR Innovation and Technology Commission (ITC) Innovation and Technology Fund (ITF), ITS/262/12: Design and Control of Flexure-Based Multi-Axis Nanopositioners for Ultra Precision Applications.

REFERENCES

[1] Howell L. Compliant Mechanisms. John Wiley and Sons Inc. New York: 2001.

[2] Vanderborght B, Albu-Schaeffer A, Bicchi A, Burdet E, Caldwell DG, Carloni R, Catalano MG, Eiberger O, Friedl W, Ganesh G, Garabini M, Grebenstein M, Grioli G, Haddadin S, Hoppner H, Jafari A, Laffranchi M, Lefeber D, Petit F, Stramigioli S, Tsagarakis NG, Damme VM, Ham VR, Visser LC, Wolf S. Variable Impedance Actuators: A Review. Robotics and Autonomous Systems. 2013; 61(12): 1601-1614.

[3] Timoshenko S. Strength of Materials II: Advanced Theory and Problems. McGraw-Hill. New York 3rd Ed.: 1955.

[4] Blanding DL. Exact Constraint: Machine Design Using Kinematic Processing. ASME Press. New York: 1999.

[5] Culpepper ML, Anderson G. Design of a Low-Cost Nano-Manipulator which Utilizes a Monolithic, Spatial Compliant Mechanism. Precision Engineering. 2004; 28(4): 469-482.